frontiers | Frontiers in Chemistry

ORIGINAL RESEARCH
published: 12 July 2022
doi: 10.3389/fchem.2022.964008

Synergistic Cr(VI) Reduction and Chloramphenicol Degradation by the Visible-Light-Induced Photocatalysis of $CuInS_2$: Performance and Reaction Mechanism

Chaosheng Zhu[1], Jingyu Li[1], Yukun Chai[1], Yongcai Zhang[2]*, Yunlin Li[1], Xiangli Zhang[3], Jin Liu[4] and Yan Li[1]*

[1]Zhoukou Key Laboratory of Environmental Pollution Prevention and Remediation, School of Chemistry and Chemical Engineering, Zhoukou Normal University, Zhoukou, China, [2]School of Chemistry and Chemical Engineering, Yangzhou University, Yangzhou, China, [3]College of Chinese Language and Literature, Zhoukou Normal University, Zhoukou, China, [4]Henan Key Laboratory of Rare Earth Functional Materials, International Joint Research Laboratory for Biomedical Nanomaterials of Henan, Zhoukou Normal University, Zhoukou, China

OPEN ACCESS

Edited by:
Yue Li,
Henan Institute of Engineering, China

Reviewed by:
Lixia Yang,
Nanchang Hangkong University, China
Dafeng Yan,
Huazhong University of Science and Technology, China

***Correspondence:**
Chaosheng Zhu
zhuchsh@foxmail.com
Yongcai Zhang
zhangyc@yzu.edu.cn

Specialty section:
This article was submitted to Nanoscience, a section of the journal Frontiers in Chemistry

Received: 08 June 2022
Accepted: 20 June 2022
Published: 12 July 2022

Citation:
Zhu C, Li J, Chai Y, Zhang Y, Li Y, Zhang X, Liu J and Li Y (2022) Synergistic Cr(VI) Reduction and Chloramphenicol Degradation by the Visible-Light-Induced Photocatalysis of $CuInS_2$: Performance and Reaction Mechanism. Front. Chem. 10:964008. doi: 10.3389/fchem.2022.964008

Despite significant scientific efforts in the field of water treatment, pollution of drinking water by toxic metal ions and synthetic organic compounds is becoming an increasing problem. The photocatalytic capabilities of $CuInS_2$ nanoparticles were examined in this study for both the degradation of chloramphenicol (CAP) and the reduction of Cr(VI). $CuInS_2$ nanoparticles were produced using a straightforward solvothermal approach and subsequently characterized by many analysis techniques. Simultaneous photocatalytic Cr(VI) reduction and CAP oxidation by the $CuInS_2$ nanoparticles under visible-light demonstrated that lower pH and sufficient dissolved oxygen favored both Cr(VI) reduction and CAP oxidation. On the basis of active species quenching experiments, the possible photocatalytic mechanisms for Cr(VI) conversion with synchronous CAP degradation were proposed. Additionally, the $CuInS_2$ retains a high rate of mixed pollutant removal after five runs. This work shows that organic contaminants and heavy metal ions can be treated concurrently by the visible-light-induced photocatalysis of $CuInS_2$.

Keywords: $CuInS_2$, Cr(VI) reduction, chloramphenicol degradation, synergistic effect, visible light photocatalysis

INTRODUCTION

Industries such as electroplating, mining, leather tanning and electronics manufacturing use large amounts of chromium compounds, leading to serious water pollution (Djellabi et al., 2019; Ge et al., 2021; Taha et al., 2021). Due to its carcinogenic, teratogenic, and transportable properties, Cr(VI) poses a substantial hazard to both the environment and human health (Wei et al., 2017; Djellabi et al., 2021; Xiong et al., 2022). Furthermore, antibiotics are used widely to treat bacterial illnesses, resulting in widespread contamination of aquatic ecosystems, including surface water and groundwater (Abdurahman et al., 2021; Bouyarmane et al., 2021; Yang et al., 2022). Because the biological toxicity of such compounds endangers the aquatic organisms and human health, a growing emphasis is being placed on their efficient removal (Qiu et al., 2022). Chloramphenicol (CAP) is a broad-spectrum antibiotic that can be used to treat a wide range of bacteria and viruses (Sun et al., 2022). Ingestion of CAP-contaminated water may lead to the growth of antibiotic-resistant bacteria and a

reduction in medullary hematopoiesis function (Yu et al., 2019). Given the inadequacy of conventional sewage treatment plants in eliminating CAP, the total removal of these antibiotic compounds from water is a major concern. In reality, heavy metals and organic contaminants coexist in the same environment quite regularly.

A variety of strategies for removing CAP and Cr(VI) have already been documented to date, including adsorption, advanced oxidation processes, and biological treatment. Because of its low cost, safety, and great efficiency, photocatalysis-based advanced oxidation technique has gotten a lot of interest in the field of organic wastewater purification (Liu et al., 2009; Han et al., 2018; Yang et al., 2021a). Several photocatalysts have also been explored for the degradation of CAP, such as jarosite, $LSCO_5$, and $SmVO_4$/g-C_3N_4 composite (Wang et al., 2021b; Leeladevi et al., 2021; Wu et al., 2022). Moreover, controlling Cr(VI) pollution through photocatalytic reduction is a viable option. A number of photocatalysts such as Fe_2O_3, Bi_2MoO_6, g-C_3N_4, SnS_2 and their composites have been shown to be capable of reducing Cr(VI) to less harmful Cr(III) under visible-light irradiation (Zhang et al., 2016; Wu et al., 2020; Liu et al., 2022b; Ge et al., 2022; Tao et al., 2022). The mechanism indicates that the conduction band and valence band of the photocatalyst play the roles of reduction and oxidation, respectively, which provides the possibility of simultaneous removal of Cr(VI) and CAP by reduction and oxidation reactions in the same photocatalytic system. Thus, the development of effective and efficient photocatalysts is required for synergistic photocatalytic reduction of Cr(VI) and degradation of CAP.

Owing to its durability, low toxicity, appropriate band gap, and good solar energy conversion efficiency, I-III-VI ternary metal sulfide semiconductors have received a lot of research attention thus far (Li et al., 2018; Zhang et al., 2021). Copper indium sulfide ($CuInS_2$) is a promising I-III-VI_2 ternary chalcopyrite material with a wide range of advantages for photocatalytic and photovoltaic applications (Yang et al., 2021b; Spera et al., 2022; Wang et al., 2022). Its conduction band is made up of In 5s orbitals, and its valence band is made up of S 3p orbitals, resulting in a small band-gap (1.53 eV for the bulk $CuInS_2$) (Chumha et al., 2020; Guo et al., 2021). It has been investigated as a photocatalyst for CO_2 reduction (Xu et al., 2018), organic pollutant degradation (Guo et al., 2019; Kaowphong et al., 2019), and nitrate ion reduction (Yue et al., 2016), etc. However, it has not been applied to the field of synergistic photocatalytic elimination of Cr(VI) and organic pollutants.

Here, $CuInS_2$ nanoparticles were prepared using a one-step hydrothermal technique, and investigated as a photocatalyst in the concurrent elimination of Cr(VI) and CAP under visible-light irradiation. Furthermore, on the grounds of different characterizations and theoretical analysis, the synergistic removal effect of pollutants and photocatalytic reaction mechanism in the Cr(VI)-CAP coexistence system were explored and discussed in detail.

EXPERIMENTAL

Materials

All the reagents (analytical grade) were purchased and used as received from Sinopharm Chemical Reagent Co., Ltd. Throughout the study, all solutions were prepared with ultrapure water (18.2 MΩ·cm).

Synthesis of $CuInS_2$

4 mmol CH_3CSNH_2, 2.0 mmol $In(NO_3)_3{\cdot}H_2O$, and 2.0 mmol $Cu(NO_3)_3{\cdot}3H_2O$ were dissolved in 40 ml anhydrous ethanol, and stirred with a magnetic stirrer for 60 min to generate a homogenous dark brown suspension. The solution was then transferred into a 100 ml Teflon-lined stainless steel autoclave and heated at 180°C for 2 h. After cooling to ambient temperature naturally, the precipitate was centrifuged, washed alternately with ethanol and water, and dried at 80°C for 24 h.

Characterization of the Synthesized $CuInS_2$

An X-ray diffractometer (XRD, PANalytical B.V.) was used to determine the phase of the as-obtained product. Field emission scanning electron microscope (FE-SEM, Japan Hitachi LTD. S4800) and transmission electron microscopy (TEM, Japanese electronics JEM-2100PLU) were used to characterize the products' microstructure. The point of zero charge (pH_{pzc}) was measured by pH drift method. X–ray photo-electron spectroscopy (XPS) was performed on a PHI 5000C ESCA System. Using a UV–Vis spectrometer (UV-2450, Shimadzu, Japan) equipped with an integrating sphere attachment and $BaSO_4$ as a reflectance standard, UV–Vis diffuse reflectance spectrum of the dry-pressed disk sample was acquired.

Photocatalytic Tests

The photocatalytic performance of the synthesized $CuInS_2$ was determined by monitoring the simultaneous photocatalytic reduction of Cr(VI) and degradation of CAP in aqueous solution under visible-light illumination. The photocatalytic experimental setup (PL-02, Beijing Precise Technology Co., Ltd.) contains a Xe arc lamp (1000 W) with a 400 nm cutoff filter, a set of cylindrical quartz reactors (80 ml), and a cold trap to keep the temperature of reaction solution constant. By dissolving $K_2Cr_2O_7$ and CAP in ultrapure water or diluting the stock solution with ultrapure water, varied concentrations of Cr(VI) and CAP solutions were obtained. The pH of the solution was adjusted to the anticipant value using a concentrated solution of NaOH or H_2SO_4. A set of tests were performed to investigate the photocatalytic Cr(VI) reduction and CAP degradation over $CuInS_2$ at various solution pHs and Cr(VI)/CAP ratios. Cr(VI) concentration was determined by the modified N, N-diphenylcarbazide spectrophotometry method (Li et al., 2021). The concentration of CAP in the solution was determined using high-resolution liquid chromatography (HPLC, Accela, Thermo Scientific, United States) equipped with an XB-C18 column (4.6250 mm, 5 m, Yuexu, China) and a UV detector. The mobile phase consisted of a 50: 50 mixture of acid aqueous solution (0.1% acetic acid) and acetonitrile. The chromatograms of CAP were achieved using a flow rate of 1.0 ml min^{-1}, an injection volume of 10 μl, and 277 nm as UV detection wavelength. The column was maintained at a temperature of 30°C. For each time measurement, approximately 4 ml of the aqueous solution was withdrawn

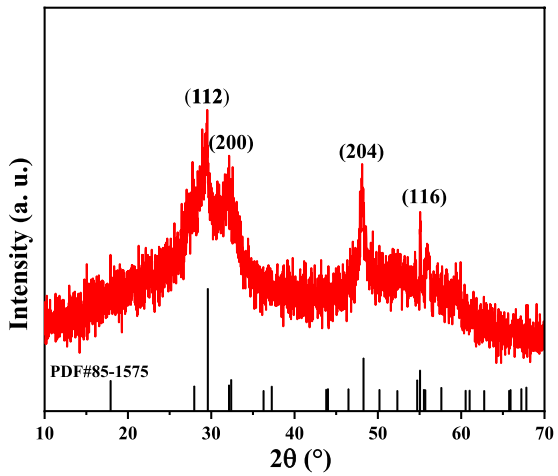

FIGURE 1 | XRD pattern of our synthesized $CuInS_2$.

from the cylindrical quartz reactors and filtered through a 0.45 nm filter to get rid of catalysts.

The Photocatalytic Reaction Kinetics Model

The photocatalytic Cr(VI) reduction and CAP degradation over $CuInS_2$ under a variety of operating conditions were studied by pseudo-first-order kinetics, which was expressed as **Eq. 1** (Mao et al., 2022):

$$\mathrm{In}\left(\frac{C_0}{C}\right) = Kt \quad (1)$$

Here, C_0 represents the concentration of Cr(VI) or CAP following the adsorption-desorption equilibrium, C represents the concentration of Cr(VI) or CAP at the irradiation time of t min, t represents the irradiation time (min), and k represents the apparent rate constant (min^{-1}).

RESULTS AND DISCUSSION

Characterization of the As-synthesized $CuInS_2$

XRD was used to determine the crystalline structure of our $CuInS_2$ product. As illustrated in **Figure 1**, there appear the diffraction peaks at 2θ = 28.1°, 32.2°, 47.1°, and 55.1°, which are respectively indexed to the (112), (200), (204), and (116) crystal planes of chalcopyrite structure $CuInS_2$ (JCPDS card No. 85–1575). The weak and wide diffraction peaks in the XRD pattern suggests that our $CuInS_2$ product has poor crystallization.

SEM and TEM were used to investigate the morphology and size of our produced $CuInS_2$. As illustrated in **Figures 2A–C**, the $CuInS_2$ sample exhibits a sheet stacking structure with dimensions ranging from 200 to 5,000 nm. The flake structure of $CuInS_2$ allows for the exposure of more active sites, which is highly advantageous for photocatalytic reactions. The EDS spectrum (**Figure 2D**) demonstrated that the prepared sample

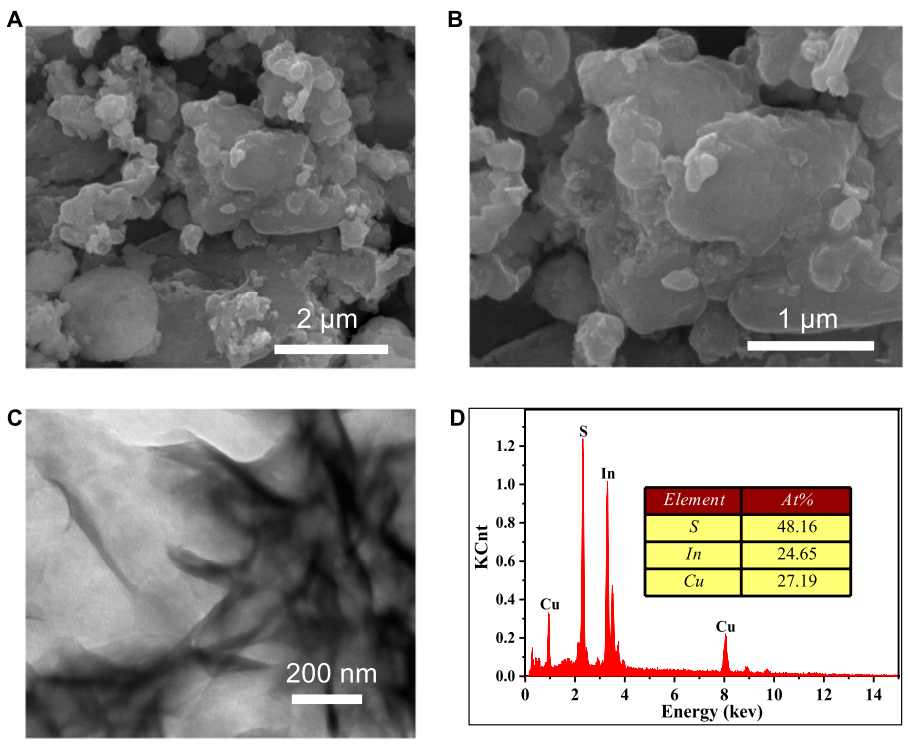

FIGURE 2 | (A,B) SEM images, **(C)** TEM image and **(D)** EDS spectrum of our synthesized $CuInS_2$.

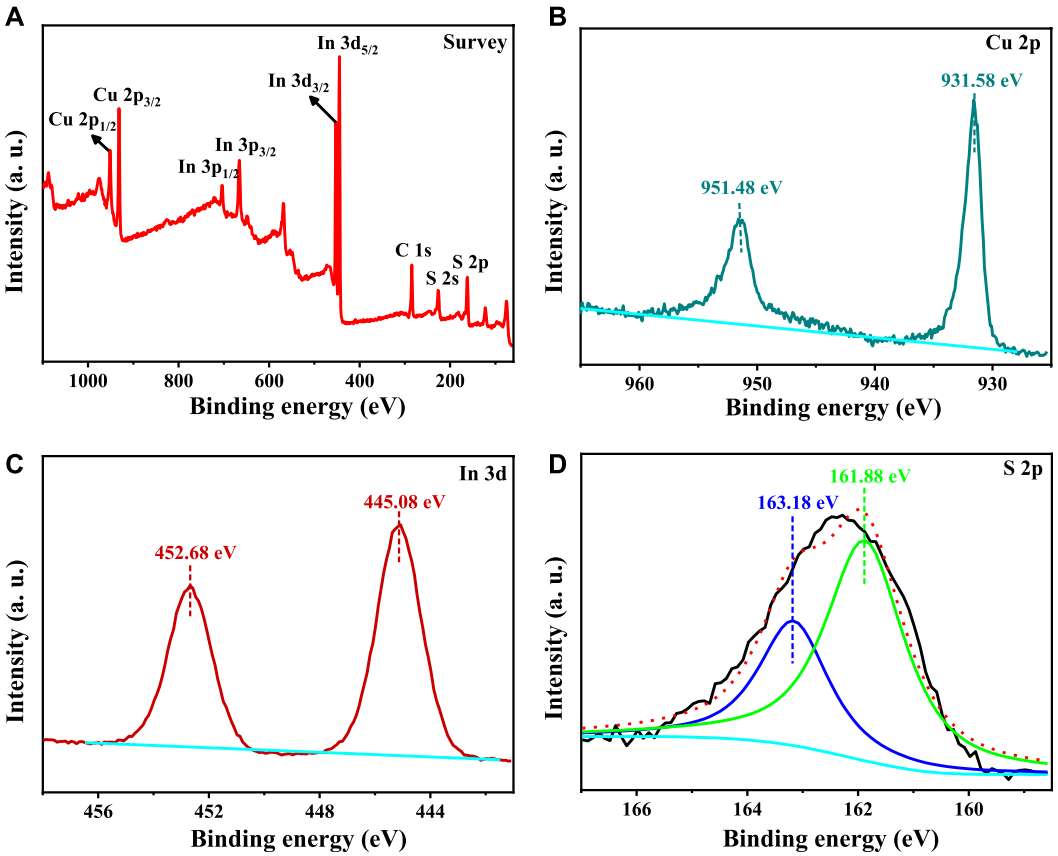

FIGURE 3 | (A) Survey, **(B)** Cu 2p, **(C)** In 3days, and **(D)** S 2p XPS spectra of our synthesized $CuInS_2$.

comprised the Cu, In, and S elements with a Cu, In, and S atomic ratio of around 1: 1: 2, confirming the formation of $CuInS_2$.

The whole XPS spectrum of our synthesized $CuInS_2$ is shown in **Figure 3A**, which reveals the existence of Cu, In, S 2p, and adventitious C in this sample. The Cu 2p XPS spectrum of our synthesized $CuInS_2$ is displayed in **Figure 3B**, which shows sharp peaks with binding energies of 951.48 eV (Cu $2p_{1/2}$) and 931.58 eV (Cu $2p_{3/2}$), respectively. There is no characteristic Cu^{2+} peak at 934.3 eV, indicating that only the Cu^{+} oxidation state is present in our synthesized $CuInS_2$ (Li et al., 2016; Yue et al., 2017). The In 3 days XPS spectrum in **Figure 3C** shows two peaks at 452.68 eV and 445.08 eV, which match with In $3d_{3/2}$ and In $3d_{5/2}$, respectively. These binding energy values indicate that In is in the In^{3+} oxidation state (Yang et al., 2015). The S 2p XPS spectrum (**Figure 3D**) was fitted into two peaks at 163.18 eV (S $2p_{1/2}$) and 161.88 eV (S $2p_{3/2}$), which are attributed to S^{2-} bonded to In or Cu in $CuInS_2$ (Liu et al., 2019; Guo et al., 2021).

The UV-Vis diffuse reflectance spectrum of our synthesized $CuInS_2$ was used to analyze its optical absorption property and band gap energy (E_g). As illustrated in **Figure 4A**, the $CuInS_2$ product demonstrates distinct absorption of visible light between 550 and 800 nm. The following formula (**Eq. 2**) can be used to estimate the E_g of the $CuInS_2$ product (Liu et al., 2022a):

$$(\alpha h\nu)^{n} = K(h\nu - Eg) \quad (2)$$

where h is the Planck's constant, α is the absorption coefficient, k is the constant, ν is the light frequency, $n = 1/2$ for an indirect band gap semiconductor, or $n = 2$ for a direct band gap semiconductor. Since absorbance (A) is directly proportional to the absorbance coefficient (α), the same E_g value can be obtained by replacing α with A. $CuInS_2$ is a direct band gap semiconductor. As shown in **Figure 4B**, by projecting the linear part of its $(Ah\nu)^2$ vs. $(h\nu)$ plot to zero, the E_g value of $CuInS_2$ is obtained to be 1.52 eV, which is close to the reported values in the literature (Guo et al., 2019; Chumha et al., 2020). This means that the $CuInS_2$ nanomaterial could be used as a visible-light-driven photocatalyst.

Effect of Solution pH on Cr(VI) Reduction and CAP Degradation

Since the solution pH can modify both the acid-base environment and the existing forms of Cr(VI), it is well established that the solution pH values exert a significant effect on photocatalytic activities (Zhang et al., 2018; Mangiri et al., 2021; Kumar et al., 2022). The effects of varying the initial pH on Cr(VI) reduction are demonstrated in **Figures 5A,B** According to **Figure 5A**, the adsorption equilibrium between catalysts and Cr(VI) can be attained after they were mixed for 40 min, because the Cr(VI) concentration did not decrease when the adsorption duration was further raised to 60 min. When the pH value decreased from 7–9

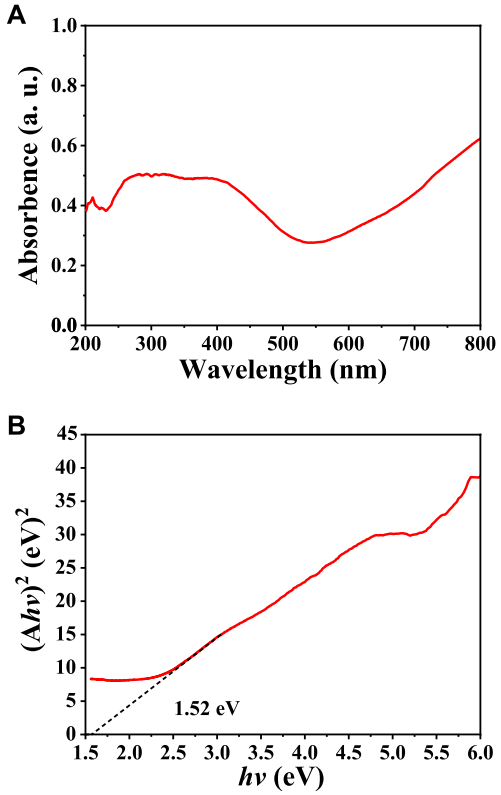

FIGURE 4 | (A) UV–Vis diffuse reflectance spectrum and **(B)** Tauc plot for obtaining the E_g value of our prepared $CuInS_2$ sample.

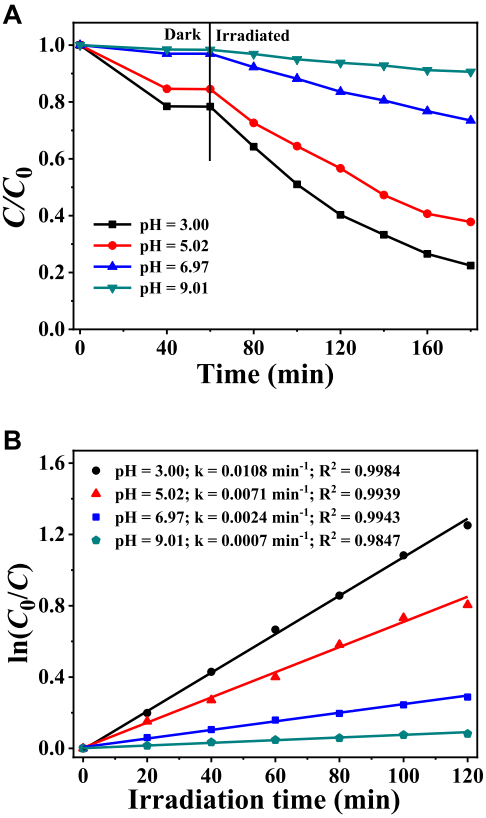

FIGURE 5 | (A) Adsorption and photocatalytic reduction of Cr(VI) over $CuInS_2$ in the mixed solution of Cr(VI) and CAP at different pH conditions **(B)** Corresponding kinetics plots for the photocatalytic Cr(VI) reduction reactions in **(A)**. ([Cr(VI)] = 10 mg/L, [CAP] = 10 mg/L, [catalyst] = 0.2 g/L).

to 5–3, the Cr(VI) adsorption capacity of $CuInS_2$ increased rapidly. The pH_{PZC} of prepared $CuInS_2$ is determined to be 5.68, so in the solutions with pH less than 5.68, the surface charges of $CuInS_2$ are positive, which is conducive to the adsorption of $Cr_2O_7^{2-}$, $HCrO_4^-$ and CrO_4^{2-} (Xu et al., 2020). When the photoreduction process began, the reduction rates of Cr(VI) significantly increased with the lengthening of the irradiation period. In addition, the decrease of the solution pH from 9.01 to 3.00 also resulted in the faster reduction rates of Cr(VI). According to **Figure 5B**, when the solution pH value is 3.0, the k value (0.0108 min^{-1}) of the photocatalytic Cr(VI) reduction over $CuInS_2$ is the largest, which is about 15.43 times as that (0.0007 min^{-1}) at pH 9.01. One reason for this is that a lower pH promotes Cr(VI) adsorption on the photocatalyst, hence accelerating photocatalytic conversion. Another possibility is that lowering the pH value of reaction solution raises the chromate reduction potential. For example, one pH unit lower results in a rise in the standard reduction potential by 0.138 V (Zhang et al., 2017). So the E(Cr(VI)/Cr(III)) value increases from 0.24 to 1.06 V as the pH of the solution decreases from 9.00 to 3.00. From the viewpoint of both kinetics and thermodynamics, the photocatalytic Cr(VI) reduction rate would be enhanced in the lower pH solution (Marinho et al., 2016; Zhang et al., 2022).

As shown in **Figure 6A**, the pH value of the solution had little effect on the adsorption of CAP by $CuInS_2$. However, the photodegradation rates of CAP can be remarkably affected by the pH of the solution. As shown in **Figure 6B**, when the solution's starting pH is 3.0, the CAP degradation rate is the fastest at the given irradiation period, and the k value is 2.9 times that of pH 9.01. The rate of CAP degradation reduced as the pH of the solution increased, indicating that the more acidic solution promotes photocatalytic CAP degradation in the mixed solution system of CAP and Cr(VI). One reason for this is that the formed $Cr(OH)_3$ tends to settle on the surface of the photocatalyst particles in neutral and alkaline solutions, reducing the available active sites of the photocatalysts and inhibiting further photocatalytic degradation of CAP and reduction of Cr(VI) (Wang et al., 2021a). The decrease in Cr(VI) conversion reduces the consumption of photogenerated electrons, causing more recombination of photogenerated electrons and holes and diminishing the photocatalytic oxidative degradation of CAP (Sun et al., 2021).

Synergy of Photocatalytic Cr(VI) Reduction and CAP Degradation Over $CuInS_2$

In the mixed solution of Cr(VI) and CAP, the possibility of simultaneous Cr(VI) reduction and CAP oxidation by the photocatalysis of $CuInS_2$ was tested. The effects of different initial

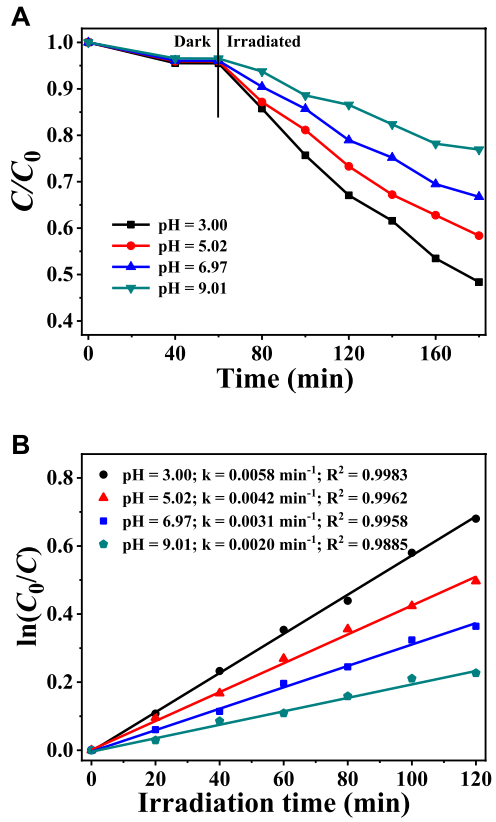

FIGURE 6 | (A) Adsorption and photocatalytic degradation of CAP over $CuInS_2$ in the mixed solution of CAP and Cr(VI) at different pH conditions **(B)** Corresponding kinetics plots for the photocatalytic CAP degradation reactions in **(A)**. ([Cr(VI)] = 10 mg/L, [CAP] = 10 mg/L, [catalyst] = 0.2 g/L).

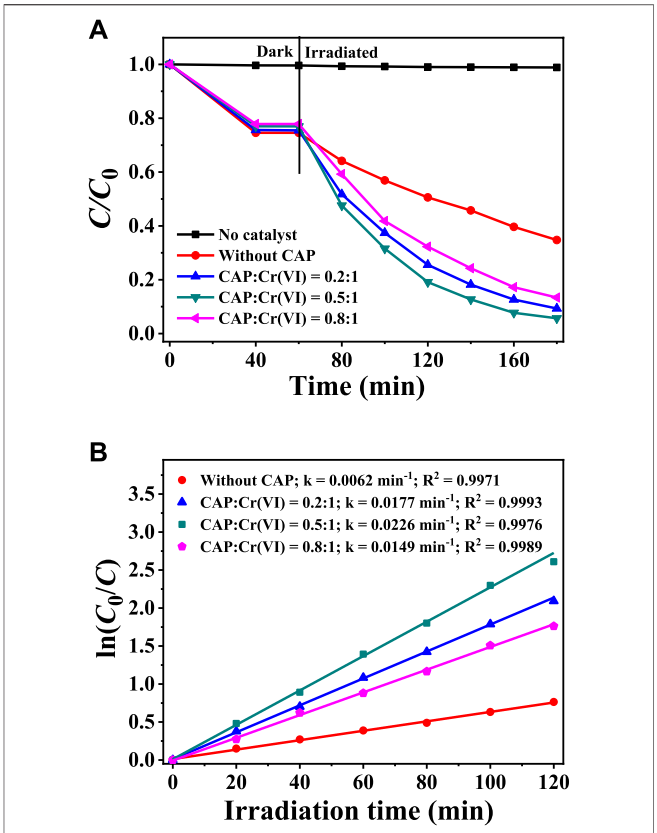

FIGURE 7 | (A) Adsorption and photocatalytic reduction of Cr(VI) over $CuInS_2$ under visible irradiation in the mixed solution with different weight ratios of Cr(VI) and CAP **(B)** Corresponding kinetics plots for the photocatalytic Cr(VI) reduction reactions in **(A)**. ([Cr(VI)] = 10 mg/L, [catalyst] = 0.2 g/L; pH = 3.0).

CAP concentrations on the photocatalytic reduction of 10 mg/L Cr(VI) over $CuInS_2$ and the corresponding kinetic behaviors were studied. As illustrated in **Figure 7A**, without $CuInS_2$, the reduction of Cr(VI) in the Cr(VI)/CAP mixed solution under visible-light irradiation can be neglected. In the mere Cr(VI) solution (without CAP), the photocatalytic reduction of Cr(VI) by $CuInS_2$ under visible-light irradiation for 120 min removed only 77.5% of Cr(VI). When the CAP/Cr(VI) ratio was 0.5: 1, over 94.3% of Cr(VI) was decreased after 120 min of visible-light irradiation, implying that the presence of CAP might increase Cr(VI) reduction by serving as a photogenerated hole scavenger. Also, it can be observed that a variation in the CAP/Cr(VI) ratio can lead to a change in the Cr(VI) reduction rate. The optimal CAP/Cr(VI) ratio is 0.5: 1, and the k value is about 3.7 times that without CAP (**Figure 7B**). This might be attributed to that when CAP concentration rises, more CAP or intermediates would be adsorbed on the $CuInS_2$ surface, potentially covering the catalyst's active sites (Cherifi et al., 2021).

Besides, the effects of varying the initial Cr(VI) concentration on the degradation of 10 mg/L CAP over $CuInS_2$ and the corresponding kinetic behaviors were examined. As shown in **Figure 8A**, CAP cannot be degraded without the presence of $CuInS_2$ catalyst, and the coexistence of Cr(VI) can effectively improve the degradation rate of CAP in the presence of $CuInS_2$ catalyst, similar to the effect of CAP on the reduction process of Cr(VI) in the mixed Cr(VI)/CAP solution under visible-light irradiation. The photodegradation kinetic behaviors of CAP over $CuInS_2$ in the solutions containing different ratios of CAP and Cr(VI) were further explored, and the results are presented in **Figure 8B**. The k values increase with decreasing the CAP/Cr(VI) ratio from 1: 1 to 1: 2 and subsequently decrease with further decreasing the CAP/Cr(VI) ratio from 1: 2 to 1: 2.5. The optimized CAP/Cr(VI) ratio is 1: 2, with a k value (0.0078 min^{-1}) for CAP degradation is about 1.5 times that of the mere CAP solution [without Cr(VI)]. The above results indicated that there is strong synergy between photocatalytic Cr(VI) reduction and CAP degradation over $CuInS_2$.

Possible Photocatalytic Mechanism

By carrying out the photocatalytic experiments with or without the addition of EDTA-Na_2 (the scavenger for photogenerated holes) as well as in air or N_2 environment, the mechanism of photocatalytic Cr(VI) conversion and CAP degradation over $CuInS_2$ was investigated. Before the start of the experiments under the N_2 environment, the reaction solution was purged with high-purity (> 99.999%) N_2 for 1 h to eliminate the dissolved O_2, and this process was maintained throughout the

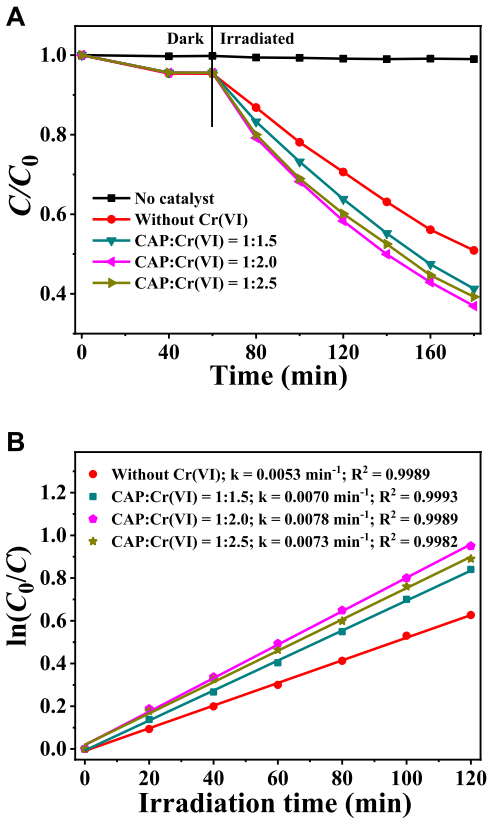

FIGURE 8 | (A) Adsorption and photocatalytic degradation of CAP over $CuInS_2$ under visible irradiation in the mixed solution with different weight ratios of Cr(VI) and CAP **(B)** Corresponding kinetics plots for the photocatalytic CAP degradation reactions in **(A)**. ([CAP] = 10 mg/L, [catalyst] = 0.2 g/L; pH = 3.0).

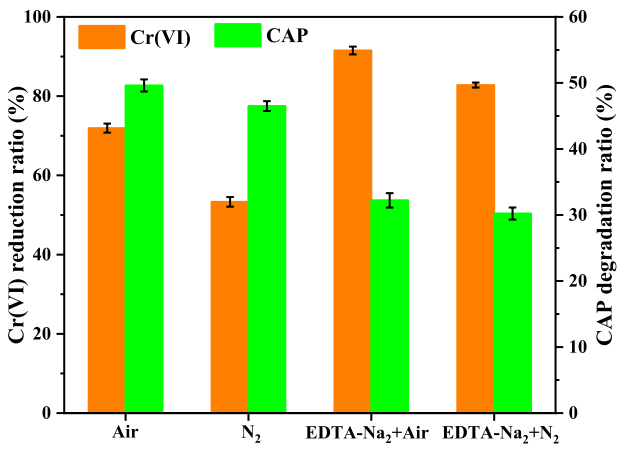

FIGURE 9 | Cr(VI) reduction and CAP degradation over $CuInS_2$ in the Cr(VI)/CAP mixed solution under air or N_2 condition as well as with or without the addition of EDTA-Na_2. ([Cr(VI)] = 10 mg/L, [CAP] = 10 mg/L, [catalyst] = 0.2 g/L, pH = 3.0, visible-light irradiation time = 120 min).

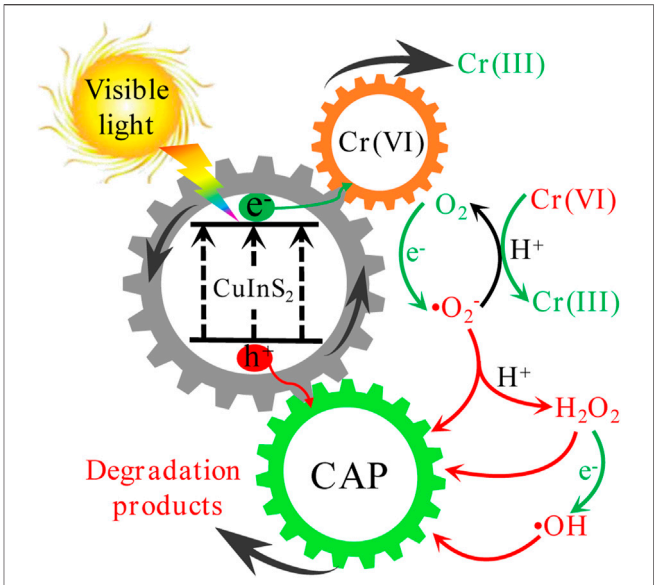

FIGURE 10 | Possible mechanisms of concurrent photocatalytic Cr(VI) reduction and CAP degradation over $CuInS_2$ under visible-light irradiation.

photocatalytic process. As shown in **Figure 9**, under visible-light illumination, the Cr(VI) conversion and CAP degradation over $CuInS_2$ in the Cr(VI)/CAP mixed solution in the air environment were more efficient than those in the N_2 environment. The suppressing impact of N_2 environment was more noticeable in the case of Cr(VI) reduction, with the Cr(VI) reduction rate dropping from 71.9% in air to 53.3% in N_2 environment. This is because that the interaction of dissolved O_2 with photogenerated electrons can produce superoxide radicals ($\bullet O_2$) (Wang et al., 2016). $\bullet O_2$ can be further converted to H_2O_2 or disproportioned to •OH, which affects the Cr(VI) reduction and CAP degradation, respectively. Furthermore, it has been shown that $\bullet O_2$ is capable of reducing Cr(VI) to Cr(V), hence improving Cr(VI) conversion (Wei et al., 2016; Deng et al., 2017). As a consequence, the rates of Cr(VI) reduction and CAP oxidation in the air environment are higher than those in the N_2 environment. As shown in **Figure 9**, the conversion proportion of Cr(VI) and the degradation proportion of CAP are 71.9% and 49.6%, respectively, without the addition of EDTA-Na_2 in the air environment under visible-light irradiation for 120 min. After adding EDTA-Na_2, the Cr(VI) conversion rose to 91.5% while the CAP degradation decreased to 32.2%. Because EDTA-Na_2 can efficiently capture photogenerated holes, so enhancing photogenerated charge carrier separation and has a promoting influence on Cr(VI) reduction (Patnaik et al., 2018). On the other hand, the addition of EDTA-Na_2 led to the decline in CAP degradation efficiency, suggesting that CAP degradation was mostly dependent on photogenerated holes (Qu et al., 2020). In the N_2 environment, the improvement in the Cr(VI) conversion and the decrease in the CAP degradation were also observed after adding EDTA-Na_2. Nevertheless, when the reaction was carried out in the N_2 environment, EDTA-Na_2 had a smaller promoting impact on the reduction of Cr(VI),

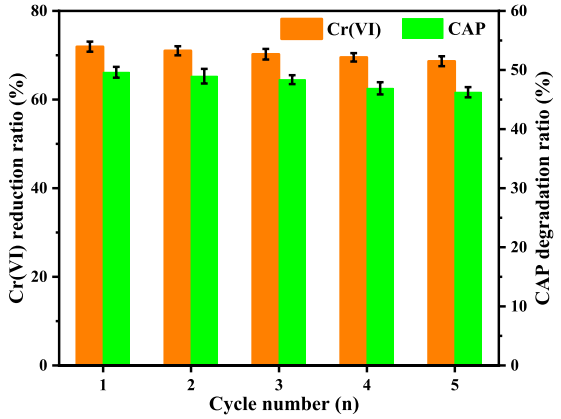

FIGURE 11 | Cycle performance of our prepared $CuInS_2$ in photocatalytic Cr(VI) reduction and CAP degradation in the Cr(VI)/CAP mixed solution. ([Cr(VI)] = 10 mg/L, [CAP] = 10 mg/L, [catalyst] = 0.2 g/L, pH = 3.0).

owing to the reduced of O_2/$\bullet O_2^-$ mediated reduction in the decrease of dissolved O_2 (Wang et al., 2016; Cherifi et al., 2021).

We postulated the possible mechanisms for the photocatalytic Cr(VI) reduction and CAP oxidation over $CuInS_2$ as shown in **Figure 10**, based on the aforesaid results. Under visible-light irradiation, photogenerated electrons (e^-) and photogenerated holes (h^+) are produced respectively in the conduction band (CB) and valence band (VB) of $CuInS_2$ (**Eq. 3**). Cr(VI) can be reduced by e^- (**Eq. 4**), while CAP can be oxidized by h^+ (**Eq. 5**). The two simultaneous processes are capable of accelerating the separation of e^- and h^+, resulting in a greater amount of e^- for Cr(VI) reduction and h^+ for CAP oxidation (Liu et al., 2022c). In addition, e^- can combine with dissolved O_2 to form $\bullet O_2^-$ (**Eq. 6**), and $\bullet O_2^-$ can reduce Cr(VI) in the presence of H^+ (**Eq. 7**) (Xia et al., 2018). Furthermore, $\bullet O_2^-$ can combine with H^+ to make H_2O_2 (**Eq. 8**), which subsequently reacts with e^- to form the powerful oxidizing $\bullet$OH (**Eq. 9**). Meantime, CAP may be oxidized by h^+ as well as the oxidizing species created, such as $\bullet O_2^-$, $\bullet$OH, and H_2O_2 (**Eq. 10**).

$$CuInS_2 + h\nu \rightarrow CuInS_2\left(h_{VB}^+ + e_{CB}^-\right) \quad (3)$$

$$Cr\,(VI) + 3e_{CB}^- \rightarrow Cr\,(III) \quad (4)$$

$$h_{VB}^+ + CAP \rightarrow \text{Degradation Products} \quad (5)$$

$$O_2 + e_{CB}^- \rightarrow \bullet O_2^- \quad (6)$$

$$Cr\,(VI) + 2\bullet O_2^- + 4H^+ \rightarrow Cr\,(III) + 2H_2O + O_2 \quad (7)$$

$$2\bullet O_2^- + 2H^+ \rightarrow O_2 + H_2O_2 \quad (8)$$

$$H_2O_2 + e_{CB}^- \rightarrow \bullet OH + OH^- \quad (9)$$

$$\bullet O_2^-/H_2O_2/\bullet OH + CAP \rightarrow \text{Degradation products} \quad (10)$$

Reusability and Stability of $CuInS_2$ Photocatalyst

The photocatalytic activity and durability of a catalyst are equally significant in practical applications. The photocatalytic endurance of $CuInS_2$ was tested by performing five successive

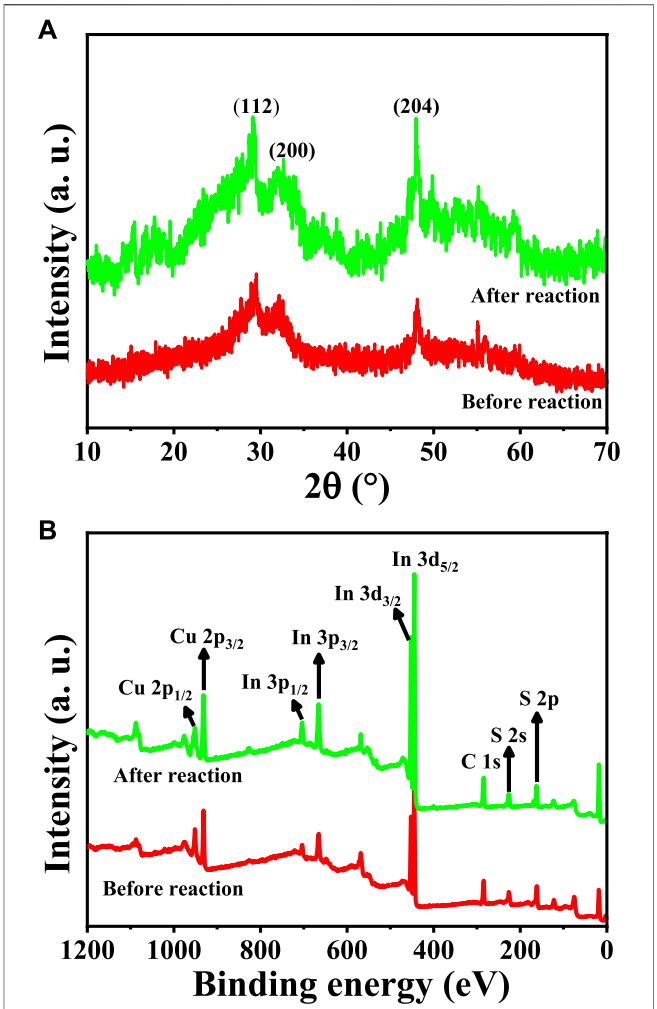

FIGURE 12 | (A) XRD patterns and **(B)** survey XPS spectra of the $CuInS_2$ before and after the cycle tests.

cycles of Cr(VI) reduction and CAP degradation in the mixed Cr(VI)/CAP solution by the same process as mentioned above, but 40 mg of photocatalyst and 200 ml of mixture were used. When each cycle ended, the photocatalyst was collected, washed and dried at 80°C for 12 h. In each cycle test, a certain amount of original Cr(VI)/CAP mixture was injected to maintain the initial concentration of pollutants. As indicated by **Figure 11**, both the Cr(VI) reduction rate and the CAP degradation rate decrease only a bit as the cycle number rises. The reduced percentage of Cr (VI) and the degraded percentage of CAP are in turn 71.9% and 49.6% in the first cycle, but still 68.7% and 46.2% in the fifth cycle, respectively. Thus, the $CuInS_2$ photocatalyst has been shown to have fair reusability for synchronous photocatalytic Cr(VI) conversion and CAP degradation. **Figures 12A,B** show the XRD patterns and survey XPS spectra of the $CuInS_2$ before and after the reuse tests. As can be seen from **Figures 12A,B**, the peak number and location of the $CuInS_2$ after the reuse tests are virtually identical to those of fresh $CuInS_2$, showing that the crystal structure, composition and elemental valence of $CuInS_2$

have little change. Accordingly, $CuInS_2$ appears to have strong stability and fair reusability, which bodes well for its future use in wastewater treatment.

CONCLUSION

$CuInS_2$ nanoparticles were synthesized by a straightforward solvothermal method and explored as a photocatalyst in the simultaneous photocatalytic Cr(VI) reduction and CAP oxidation under visible-light irradiation. It was demonstrated that lower pH and oxygenated atmosphere are advantageous for Cr(VI) reduction and CAP oxidation. The simultaneous photocatalytic reduction of Cr(VI) and oxidation of CAP over $CuInS_2$ in the mixed Cr(VI)/CAP solution had synergistic effect, which was more efficient than only the photocatalytic reduction of Cr(VI) and only the photocatalytic oxidation of CAP. Furthermore, after five runs, the $CuInS_2$ sample retains a high rate of mixed pollutant removal. The possible mechanisms for the simultaneous photocatalytic reduction of Cr(VI) and oxidation of CAP over $CuInS_2$ were proposed. The results of this work may shed light on the synergistic effect of Cr(VI) reduction and CAP oxidation on the $CuInS_2$ catalyst. This study shows that $CuInS_2$ is a potential high-performance visible-light photocatalyst for treatment of organic contaminants and heavy metal ions in water at once.

DATA AVAILABILITY STATEMENT

The original contributions presented in the study are included in the article/Supplementary Material, further inquiries can be directed to the corresponding authors.

AUTHOR CONTRIBUTIONS

Conceptualization, CZ and YZ; methodology, CZ; investigation, CZ, XZ, and JL; resources, CZ and JL; data curation, CZ and YC; writing—original draft preparation, CZ; writing—review and editing, YZ; visualization, CZ and YL; supervision, YZ and JL; funding acquisition, CZ, YL, YC, and YL. All authors have read and agreed to the published version of the manuscript.

FUNDING

This work is financially supported by Natural Science Foundation of Henan Province (No. 202300410521), the National Natural Science Foundation of China (No. 21806194), the Science and Technology Research Plan Program of Henan Province (No. 222102320328), Scientific Research and Innovation Fund for College Students of Zhoukou Normal University (Nos. ZKNUD2022010, ZKNUD2022047).

REFERENCES

Abdurahman, M. H., Abdullah, A. Z., and Shoparwe, N. F. (2021). A Comprehensive Review on Sonocatalytic, Photocatalytic, and Sonophotocatalytic Processes for the Degradation of Antibiotics in Water: Synergistic Mechanism and Degradation Pathway. *Chem. Eng. J.* 413, 127412. doi:10.1016/j.cej.2020.127412

Bouyarmane, H., El Bekkali, C., Labrag, J., Es-saidi, I., Bouhnik, O., and Abdelmoumen, H. (2021). Photocatalytic Degradation of Emerging Antibiotic Pollutants in Waters by TiO_2/Hydroxyapatite Nanocomposite Materials. *Surfaces Interfaces* 24, 101155. doi:10.1016/J.SURFIN.2021.101155

Cherifi, Y., Barras, A., Addad, A., Ouddane, B., Roussel, P., Chaouchi, A., et al. (2021). Simultaneous Photocatalytic Cr(VI) Reduction and Phenol Degradation over Copper Sulphide-Reduced Graphene Oxide Nanocomposite under Visible Light Irradiation: Performance and Reaction Mechanism. *Chemosphere* 268, 128798. doi:10.1016/J.CHEMOSPHERE.2020.128798

Chumha, N., Pudkon, W., Chachvalvutikul, A., Luangwanta, T., Randorn, C., Inceesungvorn, B., et al. (2020). Photocatalytic Activity of $CuInS_2$ Nanoparticles Synthesized via a Simple and Rapid Microwave Heating Process. *Mat. Res. Express* 7, 015074. doi:10.1088/2053-1591/AB6885

Deng, Y., Tang, L., Zeng, G., Zhu, Z., Yan, M., Zhou, Y., et al. (2017). Insight into Highly Efficient Simultaneous Photocatalytic Removal of Cr(VI) and 2,4-diclorophenol under Visible Light Irradiation by Phosphorus Doped Porous Ultrathin g-C_3N_4 Nanosheets from Aqueous Media: Performance and Reaction Mechanism. *Appl. Catal. B Environ.* 203, 343–354. doi:10.1016/J.APCATB.2016.10.046

Djellabi, R., Yang, B., Wang, Y., Cui, X., and Zhao, X. (2019). Carbonaceous Biomass-Titania Composites with TiOC Bonding Bridge for Efficient Photocatalytic Reduction of Cr(VI) under Narrow Visible Light. *Chem. Eng. J.* 366, 172–180. doi:10.1016/J.CEJ.2019.02.035

Djellabi, R., Zhao, X., Ordonez, M. F., Falletta, E., and Bianchi, C. L. (2021). Comparison of the Photoactivity of Several Semiconductor Oxides in Floating Aerogel and Suspension Systems towards the Reduction of Cr(VI) under Visible Light. *Chemosphere* 281, 130839. doi:10.1016/J.CHEMOSPHERE.2021.130839

Ge, T., Jiang, Z., Shen, L., Li, J., Lu, Z., Zhang, Y., et al. (2021). Synthesis and Application of Fe_3O_4/$FeWO_4$ Composite as an Efficient and Magnetically Recoverable Visible Light-Driven Photocatalyst for the Reduction of Cr(VI). *Sep. Purif. Technol.* 263, 118401. doi:10.1016/J.SEPPUR.2021.118401

Ge, T., Shen, L., Li, J., Zhang, Y., and Zhang, Y. (2022). Morphology-controlled Hydrothermal Synthesis and Photocatalytic Cr(VI) Reduction Properties of α-Fe_2O_3. *Colloids Surfaces A Physicochem. Eng. Asp.* 635, 128069. doi:10.1016/J.COLSURFA.2021.128069

Guo, F., Shi, W., Li, M., Shi, Y., and Wen, H. (2019). 2D/2D Z-Scheme Heterojunction of $CuInS_2$/g-C_3N_4 for Enhanced Visible-Light-Driven Photocatalytic Activity towards the Degradation of Tetracycline. *Sep. Purif. Technol.* 210, 608–615. doi:10.1016/J.SEPPUR.2018.08.055

Guo, J., Wang, L., Wei, X., Alothman, Z. A., Albaqami, M. D., Malgras, V., et al. (2021). Direct Z-Scheme $CuInS_2$/Bi_2MoO_6 Heterostructure for Enhanced Photocatalytic Degradation of Tetracycline under Visible Light. *J. Hazard. Mat.* 415, 125591. doi:10.1016/J.JHAZMAT.2021.125591

Han, J., Li, Y., Yang, L., Li, T., Luo, Y., Yang, L., et al. (2018). Mesoporous TiO_2 with WO_3 Functioning as Dopant and Light-Sensitizer: A Highly Efficient Photocatalyst for Degradation of Organic Compound. *J. Hazard. Mat.* 358, 44–52. doi:10.1016/J.JHAZMAT.2018.06.039

Kaowphong, S., Choklap, W., Chachvalvutikul, A., and Chandet, N. (2019). A Novel $CuInS_2$/m-$BiVO_4$ p-n Heterojunction Photocatalyst with Enhanced Visible-Light Photocatalytic Activity. *Colloids Surfaces A Physicochem. Eng. Asp.* 579, 123639. doi:10.1016/J.COLSURFA.2019.123639

Kumar, D. P., Seo, S., Rangappa, A. P., Kim, S., Joshi Reddy, K. A., Gopannagari, M., et al. (2022). Ultrathin Layered Zn-Doped MoS_2 Nanosheets Deposited onto CdS Nanorods for Spectacular Photocatalytic Hydrogen Evolution. *J. Alloys Compd.* 905, 164193. doi:10.1016/J.JALLCOM.2022.164193

Leeladevi, K., Vinoth Kumar, J., Arunpandian, M., Thiruppathi, M., and Nagarajan, E. R. (2021). Investigation on Photocatalytic Degradation of Hazardous Chloramphenicol Drug and Amaranth Dye by $SmVO_4$ Decorated g-C_3N_4 Nanocomposites. *Mat. Sci. Semicond. process.* 123, 105563. doi:10.1016/J.MSSP.2020.105563

Li, M., Ramachandran, R., Sakthivel, T., Wang, F., and Xu, Z. X. (2021). Siloxene: An Advanced Metal-free Catalyst for Efficient Photocatalytic Reduction of Aqueous Cr(VI) under Visible Light. *Chem. Eng. J.* 421, 129728. doi:10.1016/J.CEJ.2021.129728

Li, M., Zhao, R., Su, Y., Hu, J., Yang, Z., and Zhang, Y. (2016). Hierarchically $CuInS_2$ Nanosheet-Constructed Nanowire Arrays for Photoelectrochemical Water Splitting. *Adv. Mat. Interfaces* 3, 1600494. doi:10.1002/ADMI.201600494

Li, S., Tang, X., Zang, Z., Yao, Y., Yao, Z., Zhong, H., et al. (2018). I-III-VI Chalcogenide Semiconductor Nanocrystals: Synthesis, Properties, and Applications. *Chin. J. Catal.* 39, 590–605. doi:10.1016/S1872-2067(18)63052-9

Liu, J., Chen, H., Zhu, C., Han, S., Li, J., She, S., et al. (2022a). Efficient Simultaneous Removal of Tetracycline Hydrochloride and Cr(VI) through Photothermal-Assisted photocatalytic-Fenton-like Processes with CuOx/γ-Al_2O_3. *J. Colloid Interface Sci.* doi:10.1016/J.JCIS.2022.04.091

Liu, J., Wu, J., Wang, N., Tian, F., and Li, J. (2022b). Surface Reconstruction of BiSI Nanorods for Superb Photocatalytic Cr(VI) Reduction under Near-Infrared Light Irradiation. *Chem. Eng. J.* 435, 135152. doi:10.1016/J.CEJ.2022.135152

Liu, X., Liu, B., Li, L., Zhuge, Z., Chen, P., Li, C., et al. (2019). $Cu_2In_2ZnS_5/Gd_2O_2S$: Tb for Full Solar Spectrum Photoreduction of Cr(VI) and CO_2 from UV/vis to Near-Infrared Light. *Appl. Catal. B Environ.* 249, 82–90. doi:10.1016/J.APCATB.2019.02.061

Liu, Y., Lin, Y., Tang, J., Liu, X., Chen, L., Tian, Y., et al. (2022c). Preparation of a Coated ZH-Scheme (SnS_2@CdS)/TiO_2(001) Photocatalyst for Phenol Degradation with Simultaneous Cr(VI) Conversion. *Appl. Surf. Sci.* 574, 151595. doi:10.1016/J.APSUSC.2021.151595

Liu, Y., Zhang, Y. C., and Xu, X. F. (2009). Hydrothermal Synthesis and Photocatalytic Activity of CdO_2 Nanocrystals. *J. Hazard. Mat.* 163, 1310–1314. doi:10.1016/J.JHAZMAT.2008.07.101

Mangiri, R., Sunil kumar, K., Subramanyam, K., Ratnakaram, Y. C., Sudharani, A., Reddy, D. A., et al. (2021). Boosting Solar Driven Hydrogen Evolution Rate of CdS Nanorods Adorned with MoS_2 and SnS_2 Nanostructures. *Colloid Interface Sci. Commun.* 43, 100437. doi:10.1016/J.COLCOM.2021.100437

Mao, Y., Qiu, J., Zhang, P., Fei, Z., Bian, C., Janani, B. J., et al. (2022). A Strategy of Silver Ferrite/Bismuth Ferrite Nano-Hybrids Synthesis for Synergetic White-Light Photocatalysis, Antibacterial Systems and Peroxidase-like Activity. *J. Photochem. Photobiol. A Chem.* 426, 113756. doi:10.1016/J.JPHOTOCHEM.2021.113756

Marinho, B. A., Cristóvão, R. O., Loureiro, J. M., Boaventura, R. A. R., and Vilar, V. J. P. (2016). Solar Photocatalytic Reduction of Cr(VI) over Fe(III) in the Presence of Organic Sacrificial Agents. *Appl. Catal. B Environ.* 192, 208–219. doi:10.1016/J.APCATB.2016.03.061

Patnaik, S., Das, K. K., Mohanty, A., and Parida, K. (2018). Enhanced Photo Catalytic Reduction of Cr(VI) over Polymer-Sensitized g-C_3N_4/$ZnFe_2O_4$ and its Synergism with Phenol Oxidation under Visible Light Irradiation. *Catal. Today* 315, 52–66. doi:10.1016/J.CATTOD.2018.04.008

Qiu, Y., Lu, J., Yan, Y., Niu, J., and Duan, Y. (2022). Bismuth Molybdate Photocatalyst for the Efficient Photocatalytic Degradation of Tetracycline in Water under Visible-Light Irradiation. *Surfaces Interfaces* 31, 102009. doi:10.1016/J.SURFIN.2022.102009

Qu, Z., Liu, Z., Wu, A., Piao, C., Li, S., Wang, J., et al. (2020). Preparation of a Coated Z-Scheme and H-type $SrTiO_3$/($BiFeO_3$@ZnS) Composite Photocatalyst and Application in Degradation of 2,4-dichlorophenol with Simultaneous Conversion of Cr(VI). *Sep. Purif. Technol.* 240, 116653. doi:10.1016/J.SEPPUR.2020.116653

Spera, E. L., Pereyra, C. J., Di Iorio, Y., Berruet, M., Vazquez, M., and Marotti, R. E. (2022). Charge Dynamics in $CuInS_2$ Photovoltaic Devices with In_2S_3 as Buffer Layer. *Mat. Chem. Phys.* 282, 125871. doi:10.1016/J.MATCHEMPHYS.2022.125871

Sun, T., Su, Y., Song, H., and Lv, Y. (2022). New Advanced Oxidation Progress with Chemiluminescence Behavior Based on NaClO Triggered by WS_2 Nanosheets. *J. Hazard. Mat.* 429, 128329. doi:10.1016/J.JHAZMAT.2022.128329

Sun, Y., Xu, L., Jin, P., Bai, X., Jin, X., and Shi, X. (2021). Simultaneous Removal of Colorless Micropollutants and Hexavalent Chromium by Pristine TiO_2 under Visible Light: An Electron Transfer Mechanism. *Chem. Eng. J.* 405, 126968. doi:10.1016/J.CEJ.2020.126968

Taha, A., Da'na, E., and Hassanin, H. A. (2021). Modified Activated Carbon Loaded with Bio-Synthesized Ag/ZnO Nanocomposite and its Application for the Removal of Cr(VI) Ions from Aqueous Solution. *Surfaces Interfaces* 23, 100928. doi:10.1016/J.SURFIN.2021.100928

Tao, X., Hu, X., Wen, Z., Ming, Y., Li, J., Liu, Y., et al. (2022). Highly Efficient Cr(VI) Removal from Industrial Electroplating Wastewater over Bi_2S_3 Nanostructures Prepared by Dual Sulfur-Precursors: Insights on the Promotion Effect of Sulfate Ions. *J. Hazard. Mat.* 424, 127423. doi:10.1016/J.JHAZMAT.2021.127423

Wang, J. C., Ren, J., Yao, H. C., Zhang, L., Wang, J. S., Zang, S. Q., et al. (2016). Synergistic Photocatalysis of Cr(VI) Reduction and 4-Chlorophenol Degradation over Hydroxylated α-Fe_2O_3 under Visible Light Irradiation. *J. Hazard. Mat.* 311, 11–19. doi:10.1016/J.JHAZMAT.2016.02.055

Wang, J. W., Qiu, F. G., Wang, P., Ge, C., and Wang, C. C. (2021a). Boosted Bisphenol A and Cr(VI) Cleanup over Z-Scheme WO_3/MIL-100(Fe) Composites under Visible Light. *J. Clean. Prod.* 279, 123408. doi:10.1016/J.JCLEPRO.2020.123408

Wang, X., Xie, Y., Tong, W., Hu, W., Wang, Y., and Zhang, Y. (2021b). Photochemical Degradation of Chloramphenicol over Jarosite/oxalate System: Performance and Mechanism Investigation. *J. Environ. Chem. Eng.* 9, 104570. doi:10.1016/J.JECE.2020.104570

Wang, Y., Peng, J., Xu, Y., Zhao, R., Han, J., and Wang, L. (2022). Facile Fabrication of CdSe/$CuInS_2$ Microflowers with Efficient Photocatalytic Hydrogen Production Activity. *Int. J. Hydrogen Energy* 47, 8294–8302. doi:10.1016/J.IJHYDENE.2021.12.182

Wei, H., Hou, C., Zhang, Y., and Nan, Z. (2017). Scalable Low Temperature in Air Solid Phase Synthesis of Porous Flower-like Hierarchical Nanostructure SnS_2 with Superior Performance in the Adsorption and Photocatalytic Reduction of Aqueous Cr(VI). *Sep. Purif. Technol.* 189, 153–161. doi:10.1016/J.SEPPUR.2017.08.014

Wei, H., Zhang, Q., Zhang, Y., Yang, Z., Zhu, A., and Dionysiou, D. D. (2016). Enhancement of the Cr(VI) Adsorption and Photocatalytic Reduction Activity of g-C_3N_4 by Hydrothermal Treatment in HNO_3 Aqueous Solution. *Appl. Catal. A Gen.* 521, 9–18. doi:10.1016/J.APCATA.2015.11.005

Wu, Y., Mao, S., Liu, C., Pei, F., Wang, F., Hao, Q., et al. (2022). Enhanced Degradation of Chloramphenicol through Peroxymonosulfate and Visible Light over Z-Scheme Photocatalysts: Synergetic Performance and Mechanism Insights. *J. Colloid Interface Sci.* 608, 322–333. doi:10.1016/J.JCIS.2021.09.197

Wu, Z., He, X., Xue, Y., Yang, X., Li, Y., Li, Q., et al. (2020). Cyclodextrins Grafted MoS_2/g-C_3N_4 as High-Performance Photocatalysts for the Removal of Glyphosate and Cr(VI) from Simulated Agricultural Runoff. *Chem. Eng. J.* 399, 125747. doi:10.1016/J.CEJ.2020.125747

Xia, Q., Huang, B., Yuan, X., Wang, H., Wu, Z., Jiang, L., et al. (2018). Modified Stannous Sulfide Nanoparticles with Metal-Organic Framework: Toward Efficient and Enhanced Photocatalytic Reduction of Chromium (VI) under Visible Light. *J. Colloid Interface Sci.* 530, 481–492. doi:10.1016/J.JCIS.2018.05.015

Xiong, J., Zeng, H. Y., Chen, C. R., Peng, D. Y., Xu, S., and An, D. S. (2022). Conjugated Hollow polyaniline/$CuBi_2O_4$ Composite with Enhanced Photocatalytic Activity under Visible-Light. *Surfaces Interfaces* 29, 101804. doi:10.1016/J.SURFIN.2022.101804

Xu, F., Zhang, J., Zhu, B., Yu, J., and Xu, J. (2018). $CuInS_2$ Sensitized TiO_2 Hybrid Nanofibers for Improved Photocatalytic CO_2 Reduction. *Appl. Catal. B Environ.* 230, 194–202. doi:10.1016/J.APCATB.2018.02.042

Xu, P., Zheng, D., Xie, Z., He, Q., and Yu, J. (2020). The Degradation of Ibuprofen in a Novel Microbial Fuel Cell with PANi@CNTs/SS Bio-Anode and $CuInS_2$ Photocatalytic Cathode: Property, Efficiency and Mechanism. *J. Clean. Prod.* 265, 121872. doi:10.1016/J.JCLEPRO.2020.121872

Yang, J., Sun, J., Chen, S., Lan, D., Li, Z., Li, Z., et al. (2022). S-Scheme 1 T Phase $MoSe_2$/AgBr Heterojunction toward Antibiotic Degradation: Photocatalytic Mechanism, Degradation Pathways, and Intermediates Toxicity Evaluation. *Sep. Purif. Technol.* 290, 120881. doi:10.1016/J.SEPPUR.2022.120881

Yang, L., Guo, J., Yang, T., Guo, C., Zhang, S., Luo, S., et al. (2021a). Self-assembly Cu_2O Nanowire Arrays on Cu Mesh: A Solid-State, Highly-Efficient, and Stable Photocatalyst for Toluene Degradation under Sunlight. *J. Hazard. Mat.* 402, 123741. doi:10.1016/J.JHAZMAT.2020.123741

Yang, S., Ma, W., Zhang, Z., Zhu, J., Liu, Y., Zhang, H., et al. (2021b). Inverted Perovskite Solar Cells Based on Inorganic Hole Transport Material of $CuInS_2$ with High Efficiency and Stability. *Sol. Energy* 230, 485–491. doi:10.1016/J.SOLENER.2021.10.040

Yang, Y., Zhang, H., Zhao, Y., Song, Y., Wu, H., and Yang, S. (2015). Solvothermal Synthesis and Characterization of Carbon Nanotube–$CuInS_2$ Hybrids. *Diam. Relat. Mat.* 59, 13–20. doi:10.1016/J.DIAMOND.2015.08.015

Yu, J., Hou, X., Hu, X., Yuan, H., Wang, J., and Chen, C. (2019). Efficient Degradation of Chloramphenicol by Zero-Valent Iron Microspheres and New Insights in Mechanisms. *Appl. Catal. B Environ.* 256, 117876. doi:10.1016/J.APCATB.2019.117876

Yue, M., Wang, R., Ma, B., Cong, R., Gao, W., and Yang, T. (2016). Superior Performance of $CuInS_2$ for Photocatalytic Water Treatment: Full Conversion of Highly Stable Nitrate Ions into Harmless N_2 under Visible Light. *Catal. Sci. Technol.* 6, 8300–8308. doi:10.1039/C6CY01858K

Yue, W., Wei, F., He, C., Wu, D., Tang, N., and Qiao, Q. (2017). l -Cysteine Assisted-Synthesis of 3D In_2S_3 for 3D $CuInS_2$ and its Application in Hybrid Solar Cells. *RSC Adv.* 7, 37578–37587. doi:10.1039/C7RA05730J

Zhang, F., Zhang, Y., Wang, Y., Zhu, A., and Zhang, Y. (2022). Efficient Photocatalytic Reduction of Aqueous Cr(VI) by Zr^{4+} Doped and Polyaniline Coupled SnS_2 Nanoflakes. *Sep. Purif. Technol.* 283, 120161. doi:10.1016/J.SEPPUR.2021.120161

Zhang, F., Zhang, Y., Zhang, G., Yang, Z., Dionysiou, D. D., and Zhu, A. (2018). Exceptional Synergistic Enhancement of the Photocatalytic Activity of SnS_2 by Coupling with Polyaniline and N-Doped Reduced Graphene Oxide. *Appl. Catal. B Environ.* 236, 53–63. doi:10.1016/J.APCATB.2018.05.002

Zhang, F., Zhang, Y., Zhou, C., Yang, Z., Xue, H., and Dionysiou, D. D. (2017). A New High Efficiency Visible-Light Photocatalyst Made of SnS_2 and Conjugated Derivative of Polyvinyl Alcohol and its Application to Cr(VI) Reduction. *Chem. Eng. J.* 324, 140–153. doi:10.1016/J.CEJ.2017.05.009

Zhang, S., Zhang, Z., Si, Y., Li, B., Deng, F., Yang, L., et al. (2021). Gradient Hydrogen Migration Modulated with Self-Adapting S Vacancy in Copper-Doped $ZnIn_2S_4$ Nanosheet for Photocatalytic Hydrogen Evolution. *ACS Nano* 15, 15238–15248. doi:10.1021/ACSNANO.1C05834/ASSET/IMAGES/LARGE/NN1C05834_0007.JPEG

Zhang, Y., Zhang, F., Yang, Z., Xue, H., and Dionysiou, D. D. (2016). Development of a New Efficient Visible-Light-Driven Photocatalyst from SnS_2 and Polyvinyl Chloride. *J. Catal.* 344, 692–700. doi:10.1016/J.JCAT.2016.10.022

Conflict of Interest: The authors declare that the research was conducted in the absence of any commercial or financial relationships that could be construed as a potential conflict of interest.

Publisher's Note: All claims expressed in this article are solely those of the authors and do not necessarily represent those of their affiliated organizations, or those of the publisher, the editors and the reviewers. Any product that may be evaluated in this article, or claim that may be made by its manufacturer, is not guaranteed or endorsed by the publisher.